J. Fluid Mech. (1965), *vol.* 22, *part* 1, *pp.* 57–80
Printed in Great Britain

On the mathematics of fluidization

Part 2. Steady motion of fully developed bubbles

By J. D. MURRAY
Department of Engineering Mechanics, University of Michigan, Ann Arbor

(Received 11 August 1964)

The momentum and mass conservation equations derived in part 1 are used in the limiting case of large solids-to-fluid density ratio. Bubbles generally appear in such fluidized beds and solutions are obtained which describe the motion of the particulate and fluid phases in the presence of a fully developed bubble. The analytical solutions are shown to be in fair agreement with experiment.

1. Introduction

The notation used in this paper, part 2, is the same as that used and defined by Murray (1965) in part 1. Part 1 will be referred to as I below. A short list of symbols defined in I and used below is given at the end of this section.

In I basic general equations governing the flow régimes in a fluidized bed were derived and it was shown that such beds were unstable to small internal disturbances and in general stable to small surface oscillations.

The equations derived in I are general. In this paper we shall restrict ourselves to the case where heat and compressibility effects are absent and the density ratio $R \gg 1$. The relevant equations are those discussed in I, §2. All papers discussed here are for gas-fluidized beds in which there are no compressibility effects. This paper is the essence of an unpublished report by Murray (1963).

Empirically it appears that in beds where the ratio of the density of the solids to that of the fluid is greater than about 10, bubbles or voids of particles appear and move up through the bed. It was suggested that the internal instability observed in I gives the linearized description of the way bubbles start and move in a fluidized bed.

Bubbles appear in virtually all gas-fluidized beds. Their nature is most clearly observed by fluidizing non-porous spherical particles of equal size; diameters in the range 0·1–1·0 mm are most convenient. Glass ballotini fluidized by air is a suitable system to study. For example, ballotini of 0·5 mm fluidizes at a superficial minimum velocity of approximately 25 cm/sec; this velocity varies roughly as the square of the particle diameter.

It is virtually impossible in practice to fluidize this material throughout the bed without forming bubbles and the size and frequency of them increase with increasing gas flow rate. Bubbles generally form right at the bottom of the bed and rise at a velocity more or less the same as that found by Davies & Taylor (1950) for a gas bubble rising in a liquid. However, the velocity does depend on the shape of the particles, and air and sand (with a comparable

maximum diameter), for example, gives a velocity of rise for a bubble roughly 12% above that found for a gas bubble in a liquid. In general bubbles grow in size as they rise up through the bed. In apparatus of a size convenient to handle in the laboratory, bubble diameters range between about 2 and 20 cm.

Wace & Burnett (1961) in their paper on flow patterns in two-dimensional gas-fluidized beds have shown that the interstitial gas flow within the bed is essentially streamline in character.

Figure 1, plate 1, is a typical photograph of the motion of the particles relative to the bubble in a two-dimensional bed; the streamline character of the particulate flow is evident. The streaks across the bubble are primarily due to boundary layer effects on the walls.

The bubbles (excluding the indentation at the bottom) are essentially circular in section and virtually empty of particles. They thus represent moving regions of very high permeability which affect the otherwise uniform upward flow of the gas. Particles flow around the bubbles (see figure 1) as they rise and thereby impose extra drag forces on the nearby gas. The gas flow is thus modified both by these abrupt permeability changes in the bed and by the particle drag forces. It is, of course, primarily the gas flow and the resulting drag on the particles that causes the particular pattern of particle movement which results in a bubble passing up through the bed.

Davidson (1961) has studied the motion of a bubble by assuming Darcy's law, that the flows of the particles and of the fluid are potential flows, and that the bubble is spherical and a true void with fluid flowing through it and particles round it. Using equations based on these assumptions he obtains a solution which provides some useful qualitative results. While his approximate equations, discussed in § 2, are simple, convenient and generally adequate for most engineering purposes, they are invalid in various situations and regions of the flow field of practical interest. These are discussed below.

Recently Davidson & Harrison (1963, ch.4) have developed Davidson's (1961) original idea by implicitly including a contribution from the solids momentum in their discussion of the pressure distribution round a bubble.

Jackson (1963) (who considers three-dimensional bubbles) assumes that the rate of change of fluid momentum is negligible and obtains a similar set of equations to those used below and derived in I. He then assumes, as a first approximation, that the particle density is constant except where it appears in the drag force on the particles. Hence, by a strict analogy with the equations of motion for a bubble of gas moving up through a liquid, discussed by Davies & Taylor (1950), he assumes their solution for the particulate flow. On this assumption he finds numerically a solution for the particle density and derives resulting expressions for the various other quantities in terms of it and the assumed flow. The solutions are evaluated for the upper half-plane only, where the origin of the co-ordinates is the centre of the sphere representing the bubble. This is a first approximation in an iterative scheme (further approximations would be lengthier). From a practical point of view such a numerical procedure is restrictive if solutions are required for general bubble shapes and velocities. He deduces that the only solution, which satisfies the boundary conditions and equations,

must therefore also satisfy the equation for the bubble velocity found by Davies & Taylor (1950). Using the equations derived below, different solutions (found analytically) are possible: the assumption of the Davies–Taylor solution is unnecessary. It is found below that the velocity of rise is effectively the same as that given by the Davies–Taylor form but in certain circumstances can be higher. Accurate measurements of bubble velocity by Rowe, Partridge, Lyall & Ardran (1962) show it to be effectively the Davies–Taylor value. However, some experimental values are a little higher and in the case of sand it is in the region of 12% higher. Comparison between the solutions derived from the theory set out in this paper and available experimental evidence is made below (see also figures 2, 6, 13 and 14).

Recently Rowe, Partridge & Lyall (1964) have given a careful discussion of cloud (see §2) formation around bubbles and compare experimental results with the results given by Davidson's (1961) (and Davidson & Harrison 1963) theory and that below. They also discuss various gas transfer phenomena not yet included in the mathematical theory below.

In this paper gas-fluidized beds in which the solids-to-fluid density ratio is greater than 10 will be studied. The relevant equations are thus equations (15) from I. With these equations the flow phenomena associated with the steady motion of a fully developed bubble (such as is shown in figure 1) are studied. The method of solution is developed in §2 for the two-dimensional case where comparison with experiment is comparatively easy. In §3 a free-streamline solution is used in an attempt to explain the situation which obtains in the region behind the bubble. §4 gives the results in the corresponding three-dimensional case and comparison is made with existing experimental evidence. The results from this mathematical approach are shown to be in quantitative agreement with the experimental facts. Arguments are given from the resulting flow patterns as to the reasons for the bubble shape.

In a subsequent paper, the unsteady motion of a bubble will be discussed.

Partial list of symbols defined in I and used in II

D	$= Z_0/(1-Z_0)$
$D(Z)$	= modification to Stokes drag due to neighbouring particles
g	gravitation constant
$\mathbf{i}$	unit vector in the vertical $(x-)$ direction
p	pressure in the gas
R	$=\rho_s/\rho_f$
v_0	gas velocity in the undisturbed fluidized state
$\mathbf{v}_f$	gas velocity vector
$\mathbf{v}_s$	solids velocity vector
Z_0	unit volume fraction of particles in the undisturbed fluidized state
ρ_f	density of the gas
ρ_s	density of the solids
$\boldsymbol{\sigma}_s$	viscous stress tensor of the solids

2. Steady 'inviscid' two-dimensional bubble motion without a wake

By 'inviscid' we shall mean the flow governed by equation (15) of I with the exclusion of the viscous-stress-tensor term Z div $\boldsymbol{\sigma}_s$. The resulting equations are (1) below. Thus, *a priori* we exclude regions where there is a possible large shear or divergence of particles such as in the immediate neighbourhood of the bubble surface. As shown below, by comparison with experiment, such a restriction is not critical from an engineering point of view, at this stage.

We shall further consider only the steady motion which exists as a result of the presence in the bed of a fully developed bubble. We thus consider mainly gas-fluidized beds. The bubble is taken to be the centre of the co-ordinate system. Since the bubble moves in the direction of flow we shall adopt the usual convention by taking the x-axis in the flow direction and so the x-axis is vertical as shown in figure 9(*a*) with θ, the polar co-ordinate, being zero on the vertical x-axis. The axes here are those of part 1 rotated through $\frac{1}{2}\pi$. The governing equations (15) of I under the above conditions become

$$\left.\begin{aligned} &\operatorname{div} Z\mathbf{v}_s = 0, \quad \operatorname{div}(1-Z)\mathbf{v}_f = 0, \\ &\rho_s Z(\mathbf{v}_s.\operatorname{grad})\mathbf{v}_s = -g\rho_s Z\mathbf{i} + D(Z)(\mathbf{v}_f - \mathbf{v}_s), \quad \operatorname{grad} p = -D(Z)(\mathbf{v}_f - \mathbf{v}_s). \end{aligned}\right\} \tag{1}$$

It is convenient to introduce the non-dimensional quantities (denoted by primes) by

$$\left.\begin{aligned} &\mathbf{v}_f = v_0\mathbf{v}_f', \quad \mathbf{v}_s = v_0\mathbf{v}_s', \quad y = y'l, \quad x = x'l, \quad r = lr', \\ &p = (\rho_s Z_0 v_0^2)p', \quad Z = Z_0 Z', \quad D(Z) = (\rho_s Z_0 v_0/l)D'(Z'), \\ &F = v_0^2/gl, \quad \xi = (1-Z)/Z_0, \end{aligned}\right\} \tag{2}$$

where l is some characteristic length in the bed: in what follows it will be the bubble radius. F is a Froude number and ξ effectively the dimensionless voidage. Substitution of equations (2) into (1) gives the following dimensionless set of equations where for convenience the primes have been dropped:

$$\operatorname{div} Z\mathbf{v}_s = 0, \tag{3}$$

$$\operatorname{div} \xi\mathbf{v}_f = 0, \tag{4}$$

$$Z(\mathbf{v}_s.\operatorname{grad}\mathbf{v}_s) = -Z\mathbf{i}/F + D(Z)(\mathbf{v}_f - \mathbf{v}_s), \tag{5}$$

$$\operatorname{grad} p = -D(Z)(\mathbf{v}_f - \mathbf{v}_s). \tag{6}$$

For a given bed F is constant. In the undisturbed state far from the bubble,

$$\mathbf{v}_f = \mathbf{i}, \quad \mathbf{v}_s = 0, \quad Z = 1,$$

and (5) and (6) give

$$FD(1) = 1, \quad p = p_0 - x/F, \tag{7}$$

where p_0 is a constant.

Equations (3)–(7) will in general be sufficiently accurate for most engineering purposes where gross quantitative phenomenological features are required.

Consider, in the first instance, motion far from the bubble surface, and write

$$\left.\begin{aligned} &\mathbf{v}_f = (1-U)\mathbf{i} + \mathbf{v}_f', \quad \mathbf{v}_s = -U\mathbf{i} + \mathbf{v}_s', \\ &Z = 1 + Z', \quad p = p_0 - x/F + p', \\ &\xi = 1/D - Z', \quad U = U_B/v_0, \end{aligned}\right\} \tag{8}$$

where U_B is the dimensional velocity of rise of the bubble; this has to be determined by the analysis. In the usual way we assume that no rapid space variation in the dependent variables occurs in this region and that disturbances from the uniform state (denoted by primes) are small and tend to zero as $r \to \infty$. If we use equations (8) to linearize the convective momentum terms then, on the left of (5), the contribution to the linear equation is $-U\partial \mathbf{v}_s'/\partial x$. However, a better approximation to the non-linear convective term can be obtained following Lewis & Carrier (1949). We introduce a real constant c by writing the linearization of

$$Z(\mathbf{v}_s.\operatorname{grad})\,\mathbf{v}_s \quad \text{as} \quad -cU\partial \mathbf{v}_s'/\partial x. \tag{9}$$

The constant c (constant with respect to the independent variables but not with respect to F, U, etc.) can be chosen in any consistent way we wish to make the solution more accurate.

Equations (3)–(8) give the linearized form of the equations as

$$\operatorname{div} \mathbf{v}_s' = U\,\partial Z'/\partial x, \tag{10}$$

$$\operatorname{div} \mathbf{v}_f' = D(1-U)\,\partial Z'/\partial x, \tag{11}$$

$$cU\,\partial \mathbf{v}_s'/\partial x = Z'\mathbf{i}/F - (\mathbf{v}_f' - \mathbf{v}_s')/F - Z'D'(1)\,\mathbf{i}, \tag{12}$$

$$\operatorname{grad} p' = -Z'D'(1)\,\mathbf{i} - (\mathbf{v}_f' - \mathbf{v}_s')/F, \tag{13}$$

where $D'(1) = [\partial D(Z)/\partial Z]_{Z=1}$. From (10) to (12),

$$\frac{\partial^2 Z'}{\partial x^2} + \frac{FD'(1) + D(1-U) - U - 1}{cFU}\frac{\partial Z'}{\partial x} = 0. \tag{14}$$

Clearly the only solution (obtained by separation of variables or otherwise) of this equation for Z' which is such that $Z' \to 0$ as $r \to \infty$ is $Z' = 0$.

The solution $Z' = 0$, which implies $Z = 1$, is a valid solution of the linearized Oseen-like equations (10)–(13). Since there is a particle-density discontinuity at the bubble surface, these equations probably do not give an accurate representation of the flows in the immediate neighbourhood of the bubble. It is suggested that the effect of this discontinuity is primarily contained within a small 'boundary-layer' region not unlike the boundary layer in ordinary large-Reynolds-number flow past bodies. In view of the importance of the stress-tensor terms in the equations when Z does vary (see I) it is most likely that the full 'viscous' equations given in I are required for a study of this boundary-layer region. In this sense equations (1) are the 'inviscid' equations. It is with this concept in mind that Z is taken to be unity over the complete field of flow exterior to the bubble and we look for solutions of the 'Oseen' equations (15)–(18) which satisfy the boundary conditions in the entire flow field. To continue the analogy, it thus represents an outer flow into which the inner boundary-layer (Z-varying) solution must merge. In view of the fair experimental verification of the solutions it seems, at this stage, profitable and reasonable to study such 'inviscid' flows, including the free-streamline case in §3.

Relation (9) will now be used to replace the momentum term in (5) with no assumption of smallness in the linear form (see also Lewis & Carrier 1949). The solution $Z = 1$ is a consistent solution of the resulting set of equations and

the solutions found below are obtained using this solution. We thus have the following linear approximate equations for the flow and pressure fields:

$$\operatorname{div} \mathbf{v}_s = 0, \tag{15}$$

$$\operatorname{div} \mathbf{v}_f = 0, \tag{16}$$

$$cU\,\partial \mathbf{v}_s/\partial x = \mathbf{i}/F - (\mathbf{v}_f - \mathbf{v}_s)/F, \tag{17}$$

$$\operatorname{grad} p = -(\mathbf{v}_f - \mathbf{v}_s)/F, \tag{18}$$

where now

$$\mathbf{v}_f \to (1-U)\,\mathbf{i}, \quad \mathbf{v}_s \to -U\mathbf{i}, \quad p \to p_0 - x/F \quad \text{as} \quad r \to \infty.$$

Equations (15)–(18) are not all independent since (16), say, is obtained from the divergence of (17) and use of (15). Equations (15)–(18) represent three independent equations for $\mathbf{v}_f$, $\mathbf{v}_s$, and p. Clearly the motion is irrotational.

Note that the solution $Z' = 0$ ($Z = 1$) and the irrotationality of $\mathbf{v}_f$ and $\mathbf{v}_s$ are consistent *only* with the linearized form of the equations. If we assume that Z is constant *a priori* (Davidson 1961; Davidson & Harrison 1963) then (3)–(6), as shown below, are an inconsistent set of equations, which implies that Z constant is not a solution of the non-linear equations.† Equations (5) and (6) with Z constant give

$$p + \tfrac{1}{2}\mathbf{v}_s^2 = \text{const.},$$

along a streamline. Since there is no rotation at infinity this constant must be the same throughout the whole field. On the other hand, from (3), (4) and (6), with Z constant, p must be harmonic and so, from the last equation, $\mathbf{v}_s^2$ is harmonic, which implies that $\mathbf{v}_s$ is rotational in contradiction with the above, which, in view of the free-stream condition, is obtained only when the flow is irrotational (Beltrami fields are not of interest here).

Davidson's (1961) equations are (15), (16) and (18), which do not include a solids-momentum contribution. Davidson & Harrison (1963), however, implicitly include a solids momentum contribution in the Bernoulli equation that they assume, and which is similar to the above. They use it to some advantage in their study of the pressure distribution in the region around the bubble. However, their method is semi-empirical and within their framework the consistency problem does not arise. Their solutions do not satisfy the above equations. In fact, to be consistent with the above theory a linearized Bernoulli-type equation must be used: this is, in effect, included in (19) below.

The above set of linear equations (15)–(18) is consistent, and $Z = 1$ ($Z' = 0$) is a valid possible mathematical solution of (10)–(13). In view of the above discussion regarding possible 'boundary-layer' effects and the favourable experimental verification of the solutions below, it seems, at this stage, to be a reasonable solution to investigate.

Let $w_s(z)$, $w_f(z)$ be the complex potentials for $\mathbf{v}_s$ and $\mathbf{v}_f$, where $z = x + iy = re^{i\theta}$. Integration of (17), (18) gives $w_f(z)$, $p(z)$ in terms of $w_s(z)$ as

$$\left.\begin{aligned} w_f(z) &= z + w_s(z) - cFU[U + (dw_s(z)/dz)], \\ p(z) - p_0 &= -[w_f(z) - w_s(z)]/F. \end{aligned}\right\} \tag{19}$$

† In view of the close experimental justification of the constant Z solution, it is probably a reasonable approximate solution (away from the bubble surface) for the full equations.

The bubble shape, $w_s(z)$, and U are unknown and are part of the solution required. A possible physical approximation is that of constant pressure inside the bubble. Because of the 'free streamline' type nature of the solution it seems unlikely at this stage that this last approximation is sufficient to determine the exact analytical solution. However, by assuming a bubble shape (as do Davies & Taylor 1950), which can be obtained fairly accurately from experiment, results can be obtained for the various flow fields which are in quantitative agreement with the experimental facts. The approximation of constant pressure provides a method (cf. Davies & Taylor 1950) of finding the velocity of rise U. The fact that reasonable assumptions of bubble shapes result in flow patterns and phenomena which have fairly accurate experimental verification is a justification that such shapes do exist as assumed.

Figure 1† is typical of the particulate flow pattern relative to the bubble. Bubbles are essentially circular except for the indentation on the downstream side. The departure from the circle begins approximately at $\frac{7}{9}\pi$ from the leading edge in the two-dimensional case for most U of interest at this stage. The bubble shape does depend on the material, but this value is typical for regular particles of the order of size mentioned above. X-ray pictures of three-dimensional bubbles (unpublished work by Rowe in 1962) have shown that the shape varies with the velocity U rather more, but the departure from the sphere has not been found at less than $\frac{5}{9}\pi$ from the leading edge except with fine irregular material. This X-ray technique (Rowe *et al.* 1962) has shown that the indentation is filled with particles which form part of a wake which moves with the bubble (see figure 1). This wake frequently exhibits vortex-like characteristics not unlike those found in certain viscous flows past cylinders. Rowe has found experimentally that these 'vortices' detach themselves from the wake periodically. Thus, if we assume reasonable irrotational flows past approximate bubble shapes, equations (19) then give the corresponding fluid flows and pressure distributions.

In this paper we shall consider three cases: (i) that of a circular bubble $r = 1$, (ii) that of a two-dimensional bubble whose shape as closely resembles that of an actual bubble as may be wished, using conformal mapping, and (iii) that of a two-dimensional bubble with circular leading edge and with a cusped free-streamline wake (see §3) which more closely resembles what is observed experimentally.

Davidson (1961), Davidson & Harrison (1963) and Jackson (1963) all assume a circular bubble without a wake. Jackson's (1963) numerical solution is not carried into the neighbourhood of the wake region, but he states that the method can be so designed to do so if assumptions are made about the flow in the wake of the bubble. His numerical results cover a range given approximately by

$$-\tfrac{1}{2}\pi \leqslant \theta \leqslant \tfrac{1}{2}\pi.$$

† The streaks (particles) across the bubble are primarily due to the boundary-layer effects at the container sides. From equation (22) the absolute velocity inside the bubble is $\frac{3}{2}(1-z)+U$. If U is not large enough any particle which leaves the immediate neighbourhood of the bubble surface will tend to fall through the bubble. As it leaves the surface the drag on neighbouring particles is reduced and they will tend to follow the first particle. This is clearly a possible way by which the fingers of particles start in a bubble. These fingers are common (see, for example, figure 5(*a*), plate 2).

The flow field in the vicinity of the circular leading edge is not very sensitive to what is assumed at the trailing edge as illustrated by the examples considered below.

(i) *Circular bubble*

Here we take

$$w_s(z) = -U(z+1/z), \tag{20}$$

and (19) give

$$w_f(z) = (1-U)[z-U/(1-U)z] - cFU^2/z^2,\dagger$$
$$p(z)-p_0 = -z/F + cU^2/z^2.$$

Clearly p is not constant on $|z| = 1$ for any value of c. However, if we require p to be constant in the vicinity of the leading edge we can expand p in terms of θ about $\theta = 0$ and require the θ^2 term to be zero (cf. Davies & Taylor 1950). This gives

$$U = \tfrac{1}{2}(cF)^{-\frac{1}{2}}, \tag{21}$$

or in dimensional form

$$U_B = \tfrac{1}{2}(gl/c)^{\frac{1}{2}},$$

and from above

$$\left.\begin{aligned} w_f(z) &= (1-U)[z-U/(1-U)z] - 1/4z^2, \\ p(z)-p_0 &= -z/F + 1/4Fz^2. \end{aligned}\right\} \tag{22}$$

Equation (21) gives U, the dimensionless bubble velocity, as a function of c and F. The former may be chosen in any way we wish. If $c = 1$ (the normal Oseen approach) (21) reduces to the same velocity of rise as for a bubble of gas rising in a liquid found by Davies & Taylor (1950). Lewis & Carrier (1949) suggest certain mathematical methods; for example, substituting the solutions obtained into the original correct equations and taking some simple average of the difference between these and the approximate equations. For example,‡ we may require

$$\int_1^\infty z\left[\frac{dw_s(z)}{dz} + cU\right]\frac{d}{dz}\left[\frac{dw_s(z)}{dz}\right]dz = 0,$$

where $w_s(z)$ is given by (20). This gives $c = \frac{2}{3}$. An empirical method would be to determine experimentally accurate bubble velocity and thereby assign c. Figure 2 shows U against $1/F$ for various c as compared with the available experimental data. (A plot of c for various F and U found experimentally for three-dimensional bubbles shows that c for a given material is effectively a function of F only.)

From (22) the fluid flow field is clearly different for $U > 1$ and $U < 1$. Figures 3, 4 illustrate this difference. From (22) the stream function ψ_f is given by

$$\psi_f = (1-U)\sin\theta\{r + U/(1-U)r\} + \sin 2\theta/4r^2. \tag{23}$$

The distinctive feature of the fluid flow when the bubble rises faster than the free stream interstitial velocity of the fluid ($U > 1$) is shown by the $\psi_f = 0$ streamline which separates the main body of fluid flow from a region of circulating fluid. This cloud moves with the bubble and is slightly ahead of the bubble. This circulating cloud was first pointed out by Davidson (1961), but his solution

† Note that in the limit $U \to 0$ we get the simple undisturbed uniform state.

‡ If the original equations only are weighted with *any* factor, $c = \frac{1}{2}$.

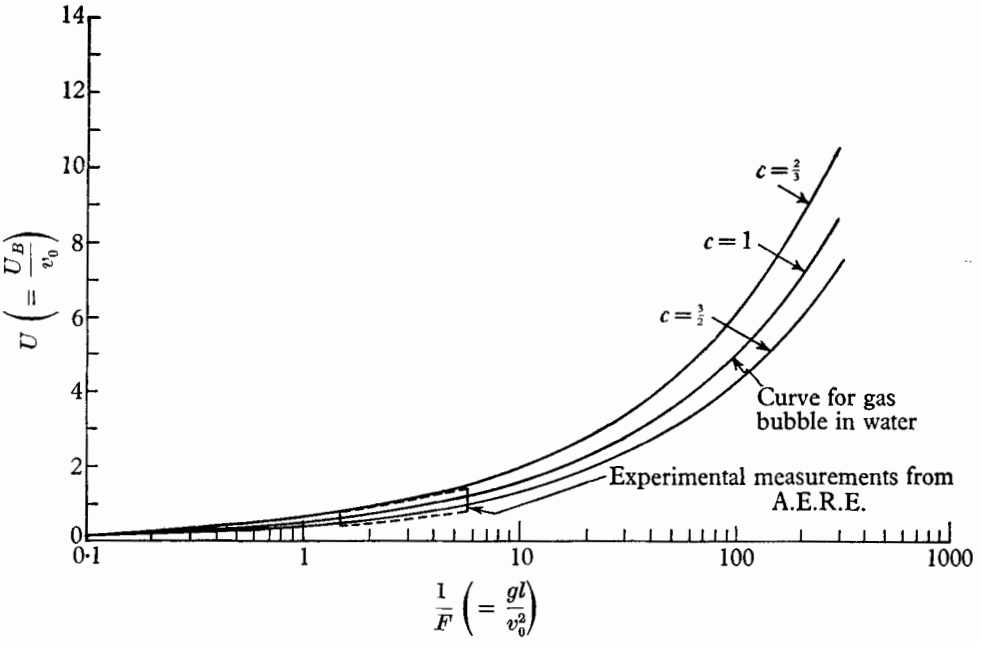

FIGURE 2. Bubble velocity against the Froude number (two-dimensional). Experiments: ballotoni–air system, $R = O(10^3)$.

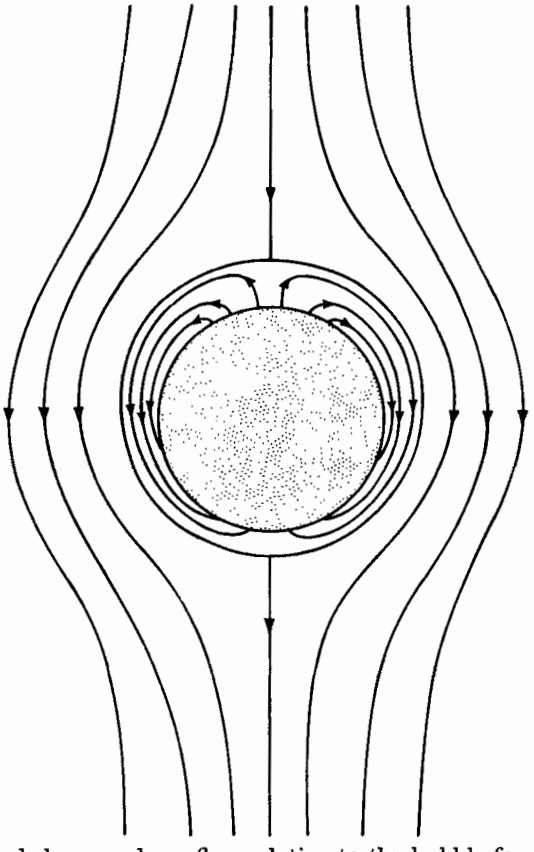

FIGURE 3. Cloud shape and gas flow relative to the bubble for $U > 1(\doteqdot 2{\cdot}4)$. (two-dimensional).

is symmetrical about the x-axis. Jackson's (1963) numerical solution (for the three-dimensional bubble) also illustrates the asymmetry discussed above. Figures 5 (a) and (b), plates 2 and 3, show this cloud in the case of a gas-fluidized bed when a puff of nitrogen dioxide is introduced with the bubble at injection. The tail of nitrogen dioxide is partially a result of the difficulty in stopping the nitrogen dioxide at exactly the correct time. There will also be some diffusion

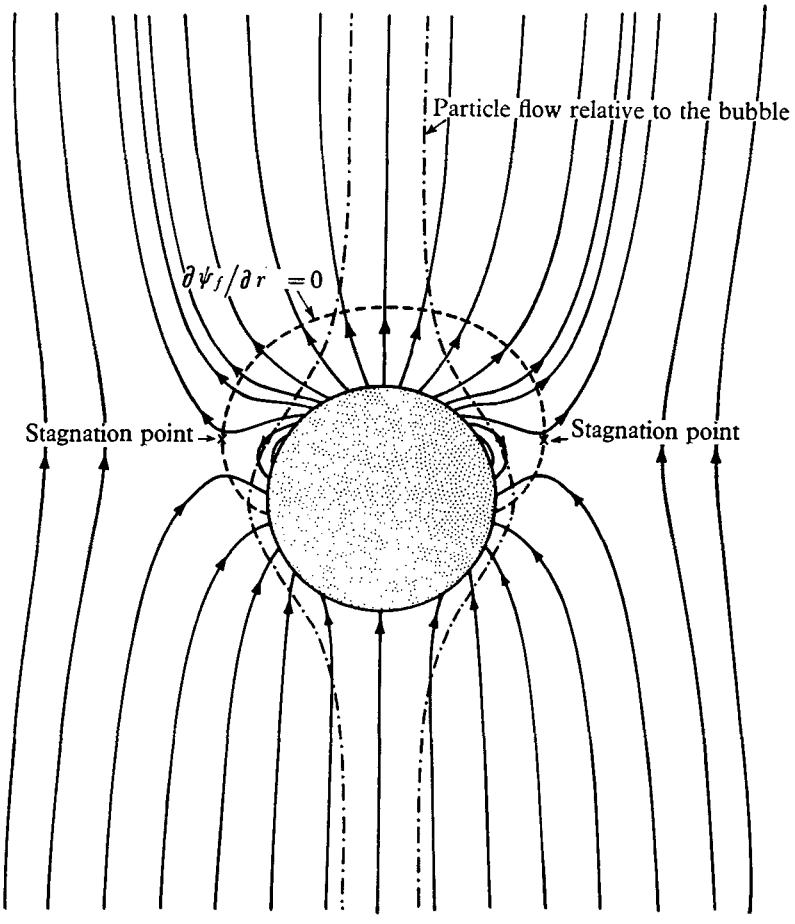

FIGURE 4. Gas flow relative to the bubble for $U < 1$ ($\doteqdot 0{\cdot}6$) (two-dimensional).

from the cloud which will move into the region immediately below the bubble and cloud. It also appears that sections of the cloud are sometimes 'cut off' and these also move into the wake as in figure 5 (b) (see §3).

In the $U < 1$ case the effect of the particle flow on the gas is effectively to increase the apparent region of the void from the point of view of flow through it as is evident from the dashed line in figures 4 and 8.

A measurable quantity experimentally, and one of practical engineering importance for the knowledge of gas movement and particle contact, is the maximum width d of the cloud. In two-dimensional bubbles the easiest accurate

experimental measurement of the cloud is the leading edge distance from the bubble centre. It is useful to know the shape of the cloud and volume of gas carried by it. From equation (23) when $\psi_f = 0$ the maximum diameter d is given by $d = (2r\sin\theta)_{\max.}$, where $\cos\theta = 2[(U-1)r^3 - Ur]$. (24)

A fair approximation to d is given by putting $\theta = \frac{1}{2}\pi$ in the second of equations (24) to give $d_{\text{approx.}} = [2r]_{\theta=\frac{1}{2}\pi} = [U/(U-1)]^{\frac{1}{2}}$.

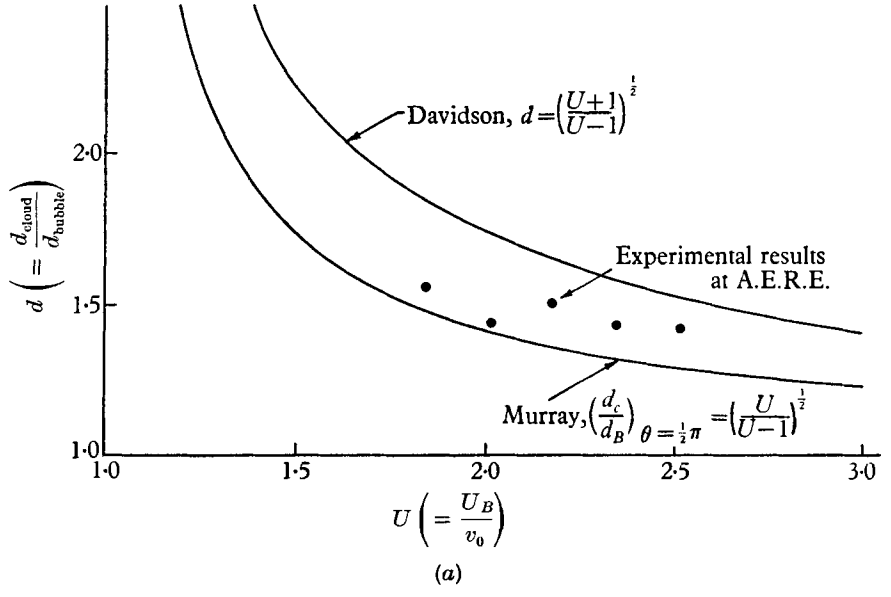

(*a*)

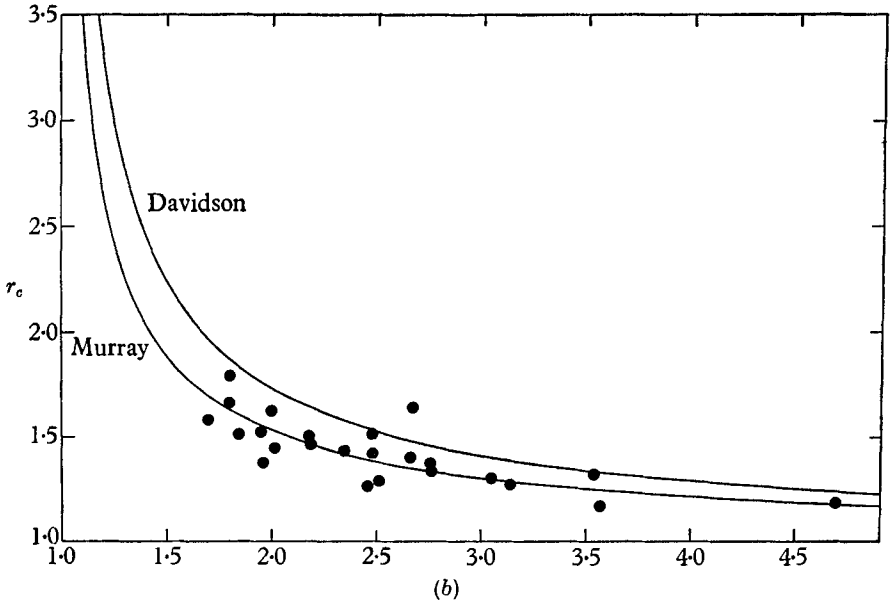

(*b*)

FIGURE 6(*a*). Ratio of cloud to bubble diameter against U (>1) (two-dimensional). (*b*) Cloud to bubble comparison at leading edge against U (>1) (two-dimensional). Ballotini (ρ_s = 2·96 g/cm³)–air experimental results at A.E.R.E.

The ratio of the distance of the cloud leading edge to the distance of the bubble leading edge from the origin is r_c, where from (23)

$$2[(U-1)r_c^3 - Ur_c] - 1 = 0. \tag{25}$$

Note that $U > 1$ for any meaning. Figures 6(*a*) and (*b*) show d against U and r_c against U respectively together with Davidson's (1961) curves and the available experimental points given by Rowe (1962). Experimentally d is less easily defined and measured than r_c.

(ii) *Kidney-shaped bubble*

If a circular bubble is introduced into the bed, the fluid flow tends to carry particles into the lower section of the bubble and the bubble quickly acquires the characteristic kidney shape shown in practically all pictures of bubbles in a fluidized bed. Initial motions when a circular bubble is introduced into a bed will be discussed in a further paper.

We now consider the irrotational flow past an actual bubble shape where we assume there is no wake. The case when there is a wake, although more realistic, is more complicated and is discussed in §3. The following mapping in slightly different form has also been applied by Collins (1965) to Davidson's (1961) theory. Collins (1965) also considers the case when there are walls present.

The conformal mapping of the circle $|\zeta| = 1$ in the ζ-plane by

$$z = \zeta + b - e^2/(\zeta + b) \tag{26}$$

gives a bubble shape which closely resembles that which is found in practice and illustrated in figure 1, if the values of b and e are

$$b \doteqdot 0{\cdot}714, \quad e \doteqdot 0{\cdot}286. \tag{27}$$

Figures 7 and 8 illustrate the improved bubble shape. Thus, the particulate flow now to be used in (19) is given by

$$w_s(z) = -\tfrac{1}{2}U[z - 2b + \{z^2 + 4e^2\}^{\frac{1}{2}} + 4/(z - 2b + \{z^2 + 4e^2\}^{\frac{1}{2}})], \tag{28}$$

with the values in (27) giving a shape representative of actual bubbles. As in §2(i) above we express the condition that $p(z)$ from (19) with $w_s(z)$ from (28) is constant in the vicinity of the leading edge on the bubble surface. This gives

$$U^2 = A/cF, \tag{29}$$

where $$A = \frac{0{\cdot}25[\{(1+b)^2+e^2\}/(1+b)^2]^2 - 0{\cdot}5\,e^2[(1+b)^2+e^2]/(1+b)^5}{1 - 2e^2/(1+b)[(1+b)^2+e^2]}.$$

For most b and e of interest, that is, in the neighbourhood of 0·7 and 0·3 respectively, $A \doteqdot 0{\cdot}25$, the value in case (i). Thus, the fluid flow is given by

$$w_f(z) = z + w_s(z) - \frac{0{\cdot}25}{U}\left[\frac{dw_s(z)}{dz}\right] + U, \tag{30}$$

where $w_s(z)$ is given by (28). Figures 7, 8 illustrate the respective flow fields

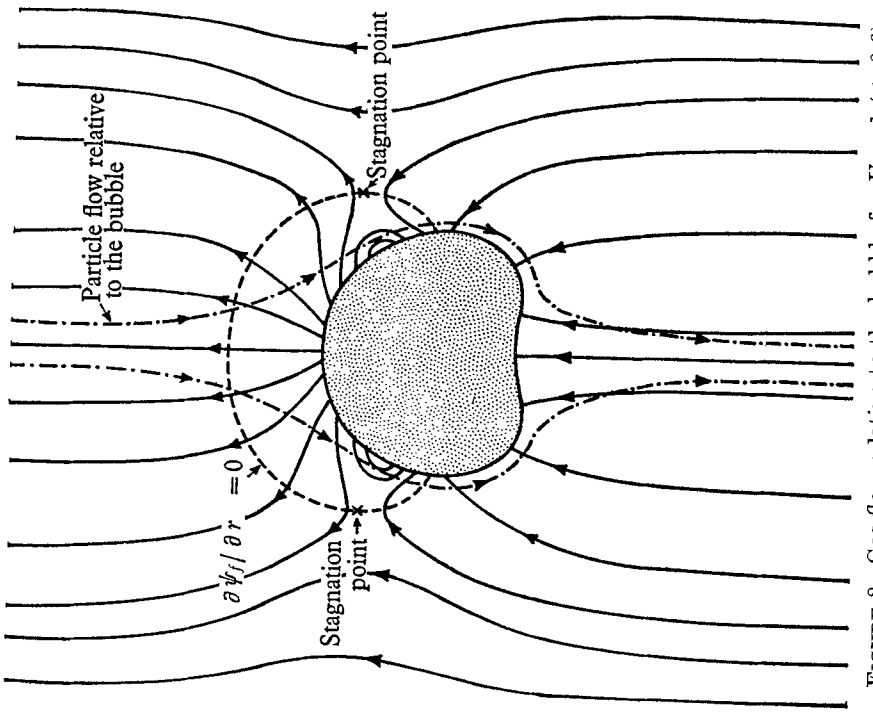

FIGURE 8. Gas flow relative to the bubble for $U < 1$ ($\doteqdot 0{\cdot}6$) (two-dimensional).

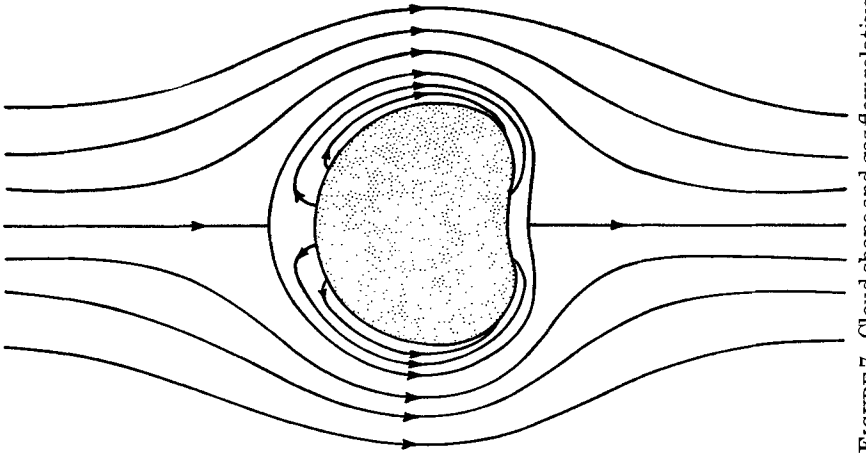

FIGURE 7. Cloud shape and gas flow relative to the bubble for $U > 1$ ($\doteqdot 2{\cdot}4$) (two-dimensional).

for $U > 1$ and $U < 1$ from (28) and (30). The cloud to bubble comparison ratios are practically the same.

Although such mappings may be used to obtain more realistic bubble shapes such refinements give only marginal improvements since of prime importance is the wake, which cannot be treated by any such mapping.

3. Fully developed bubble with a cusped free-streamline wake

At some stage between when a circular bubble is introduced into a bed and when it has developed its final kidney shape, a wake will form. From experimental evidence from X-ray pictures (Rowe, unpublished) such a wake is closed and cusped behind the bubble.

Figure 1, in fact, also illustrates its presence. In this section we shall find the solids flow past a bubble of circular shape with a cusped free streamline enclosing the wake and accordingly derive some of the fundamental features of the fluid flow resulting. On the free streamline v_s is taken to be constant. Such a configuration gives a flow which suggests explanations for some of the physical phenomena observed in practice in the wake.

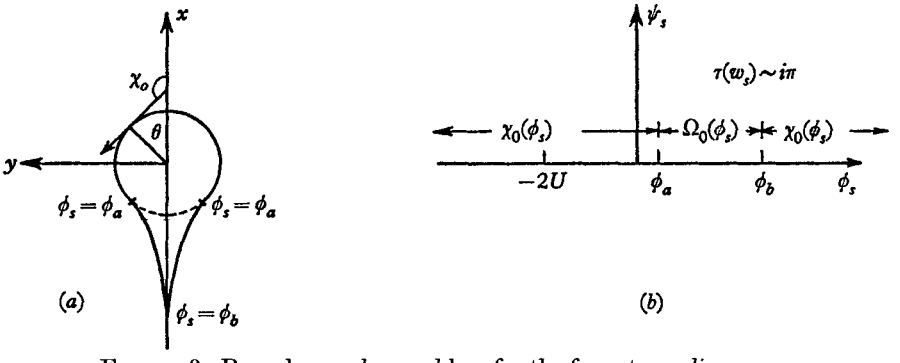

FIGURE 9. Boundary value problem for the free-streamline case. (*a*) z-plane; (*b*) w_s-plane.

We now introduce the Chaplygin function

$$\tau(w_s) = \log U\,dz/dw_s = \Omega(\phi_s, \psi_s) + i\chi(\phi_s, \psi_s), \tag{31}$$

where ϕ_s is the scalar potential, $\Omega = \log U/v_s$ and χ is the angle $\mathbf{v}_s$ makes with the positive x-axis. $\tau(w_s)$ is an analytic function of w_s and so

$$\frac{\partial^2\Omega}{\partial\phi_s^2} + \frac{\partial^2\Omega}{\partial\psi_s^2} = 0, \quad \frac{\partial^2\chi}{\partial\phi_s^2} + \frac{\partial^2\chi}{\partial\psi_s^2} = 0. \tag{32}$$

$\psi_s = 0$ includes the circular section of the bubble and the cusped free streamline. If the point of separation $\phi_s = \phi_a$ is specified and $\phi_s = \phi_b$ is the free streamline cusp, then χ is given on $\psi_s = 0$ for $-\infty \leqslant \phi_s \leqslant \phi_a$, $\phi_b \leqslant \phi_s$ and $\Omega = \Omega_s$, a constant, on the free streamline; that is, for $\phi_a \leqslant \phi_s \leqslant \phi_b$. Ω_s and ϕ_b are given by the solution and cannot be assigned. Figure 9 (*a*) illustrates the situation in the z-plane. Although χ is not known as a function of ϕ_s on $\psi_s = 0$ (but only as a func-

tion of x, y) we assume as a first approximation that $\chi(\phi_s, 0)$ and ϕ_s are related as if it were simple potential flow past a circular cylinder. Thus,

$$\phi_s = -2U\cos\theta \quad \text{on} \quad r = 1.$$

Write
$$\xi = \phi_s/2U, \tag{33}$$
which gives

$$\left.\begin{aligned}\chi(\phi_s, 0+) = \chi_0(\xi) &= \pi && \text{for} \quad -\infty \leqslant \xi \leqslant -1-0\\ &= \pi - \sin^{-1}\xi && \text{for} \quad -1+0 \leqslant \xi \leqslant \xi_a\\ &= ? && \text{for} \quad \xi_a < \xi < \xi_b\\ &= \pi && \text{for} \quad \xi_b \leqslant \xi,\end{aligned}\right\} \tag{34}$$

where χ_0 is defined by (34) and the lower half of the z-plane is taken as the positive half of the w_s-plane. Further,

$$\left.\begin{aligned}\Omega(\phi_s, 0+) = \Omega_0(\xi) &= \Omega_s, \text{ a constant for } \xi_a \leqslant \xi \leqslant \xi_b,\\ &= ? \quad \text{for all other } \xi.\end{aligned}\right\} \tag{35}$$

The problem is to find a solution for $\tau(w_s)$ given by (31) with Ω and χ satisfying (32) and with boundary conditions (34), (35) and (36) below, namely,

$$\tau(w_s) \sim i\pi \quad \text{for} \quad w_s \text{ large.} \tag{36}$$

Figure 9 (*b*) illustrates the w_s-plane boundary-value problem.

The standard solution to this problem is

$$\tau(w_s) = C(w_s)\left[\frac{1}{\pi}\left\{\int_{-\infty}^{\xi_a} + \int_{\xi_b}^{\infty}\right\}\chi_0(t)\frac{A(t)}{t - w_s/2U}dt + \frac{\Omega_s}{\pi}\int_{\xi_a}^{\xi_b}\frac{B(t)}{t - w_s/2U}dt\right], \tag{37}$$

where $A(t) = \left(\dfrac{t-\xi_b}{t-\xi_a}\right)^{\frac{1}{2}}$, $B(t) = \left(\dfrac{\xi_b - t}{t-\xi_a}\right)^{\frac{1}{2}}$, $C(w_s) = \left(\dfrac{w_s/2U - \xi_a}{w_s/2U - \xi_b}\right)^{\frac{1}{2}}$

It is to be understood that all integrals in this section are taken as the Cauchy Principal values as the need arises. Woods (1961) has considered more general mixed boundary-value problems (which include the above), but great care must be exercised in choosing the constants from physical reasoning to obtain a solution comparable to (37). It is shown below that $\tau(w_s)$ in (37) satisfies the boundary conditions. Equation (37), with χ_0 from (34), gives

$$\tau(w_s) = C(w_s)\left[\left\{\int_{-\infty}^{\xi_a} + \int_{\xi_b}^{\infty}\right\}\frac{A(t)}{t - w_s/2U}dt - \frac{1}{\pi}\int_{-1}^{\xi_a} A(t)\frac{\sin^{-1}t}{t - w_s/2U}dt + \frac{\Omega_s}{\pi}\int_{\xi_a}^{\xi_b}\frac{B(t)}{t - w_s/2U}dt\right],$$

which gives

$$\tau(w_s) = i\pi + \Omega_s[1 - C(w_s)] - \frac{C(w_s)}{\pi}\int_{-1}^{\xi_a} A(t)\frac{\sin^{-1}t}{t - w_s/2U}dt. \tag{38}$$

Since the wake is closed $\tau(w_s)$ must satisfy a closure condition which from (31) may be written as requiring

$$\tau(w_s) \sim i\pi + O(1/w_s^2) \text{ for large } w_s. \tag{39}$$

For large w_s, from above, we get

$$\tau(w_s) \sim i\pi - \tfrac{1}{2}\Omega_s(\xi_b - \xi_a)\frac{2U}{w_s} + \frac{2U}{w_s}\frac{1}{\pi}\int_{-1}^{\xi_a} A(t)\sin^{-1}t\,dt + O(1/w_s^2)$$
$$\sim i\pi + O(1/w_s^2),$$

provided the following obtains:

$$\Omega_s = \frac{2}{\pi(\xi_b - \xi_a)}\int_{-1}^{\xi_a} A(t)\sin^{-1}t\,dt. \tag{40}$$

If we now let $w_s/2U \to \xi + i(0+)$ then, since $0 > \arg C(w_s) \geqslant -\pi/2$, we get

$$\left.\begin{aligned}\lim_{w_s/2U\to\xi+i(0+)} C(w_s) &= -i/B(\xi), \quad \text{for} \quad \xi_a < \xi < \xi_b,\\ &= 1/A(\xi), \quad \text{for} \quad \xi < \xi_a \quad \text{or} \quad \xi > \xi_b.\end{aligned}\right\} \tag{41}$$

From the Plemelj formulae we obtain

$$\left.\begin{aligned}&\lim_{w_s/2U\to\xi+i(0+)} \frac{1}{\pi}\int_{-1}^{\xi_a} A(t)\frac{\sin^{-1}t}{t - w_s/2U}\,dt\\ &\quad = iA(\xi)\sin^{-1}\xi + \frac{1}{\pi}\int_{-1}^{\xi_a} A(t)\frac{\sin^{-1}t}{t-\xi}dt \quad \text{if} \quad -1 < \xi < \xi_a,\\ &\quad = \frac{1}{\pi}\int_{-1}^{\xi_a} A(t)\frac{\sin^{-1}t}{t-\xi}dt \quad \text{if} \quad \xi < -1 \quad \text{or} \quad \xi > \xi_a.\end{aligned}\right\} \tag{42}$$

Thus, from (38), (41) and (42) we get

$$\lim_{w_s/2U\to\xi+i(0+)} \tau(w_s) = \Omega_0(\xi) + i\,\chi_0(\xi)$$
$$= \Omega_s + i\left[\pi + \Omega_s/B(\xi) + \frac{1}{\pi B(\xi)}\int_{-1}^{\xi_a} A(t)\frac{\sin^{-1}t}{t-\xi}dt\right], \quad \text{for} \quad \xi_a < \xi < \xi_b, \tag{43}$$

$$= \Omega_s[1 - 1/A(\xi)] - \frac{1}{\pi A(\xi)}\int_{-1}^{\xi_a} A(t)\frac{\sin^{-1}t}{t-\xi}dt + i\begin{cases}\pi - \sin^{-1}\xi, & \text{for} \quad -1 < \xi < \xi_a,\\ \pi, & \text{for} \quad \xi < -1 \quad \text{or} \quad \xi_b < \xi.\end{cases} \tag{44}$$

From (38) there is a singularity at $\xi = \xi_b$ unless Ω_s and ξ_b are such that

$$\Omega_s = \frac{1}{\pi}\int_{-1}^{\xi_a} \frac{\sin^{-1}t\,dt}{(\xi_a - t)^{\frac{1}{2}}(\xi_b - t)^{\frac{1}{2}}}. \tag{45}$$

From (43) or (38) a little manipulation shows that

$$\lim_{\xi\to\xi_a+} \frac{1}{\pi B(\xi)}\int_{-1}^{\xi_a} A(t)\frac{\sin^{-1}t}{t-\xi}dt = -\sin^{-1}\xi_a.$$

From equation (44) there is a singularity in $\Omega_0(\xi)$ as $\xi \to -1$, since with

$$\xi = -1 + \epsilon, \quad |\epsilon| \ll 1,$$

$$-\frac{1}{\pi A(\xi)}\int_{-1}^{\xi_a} A(t)\frac{\sin^{-1}t}{t-\xi}dt \approx O(-\tfrac{1}{2}\log\epsilon).$$

From (31) this gives a half-power singularity in $|\mathbf{v}_s|$ of the form

$$v_s \approx U|\phi_s/2U+1|^{\frac{1}{2}} \quad \text{as} \quad \phi_s \to -2U,$$

as it must at the front stagnation point.

Thus, (38) gives Ω and χ for any w_s and U. On the free streamline $\psi_s = 0$, (43) gives

$$\chi_0(\xi) = \pi + \frac{\Omega_s}{B(\xi)} + \frac{1}{\pi B(\xi)} \int_{-1}^{\xi_a} A(t) \frac{\sin^{-1} t}{t-\xi} dt\dagger, \quad \text{for} \quad \xi_a < \xi < \xi_b, \tag{46}$$

and on $\psi_s = 0$ other than on the free streamline (44) gives

$$\Omega_0(\xi) = \Omega_s[1 - 1/A(\xi)] - \frac{1}{\pi A(\xi)} \int_{-1}^{\xi_a} A(t) \frac{\sin^{-1} t}{t-\xi} dt,$$
$$\text{for} \quad \xi_b < \xi \quad \text{and} \quad -\infty < \xi < \xi_a, \tag{47}$$

where ξ_a is specified and ξ_b and Ω_s are given by (40) and (45).

Equations (44) and (47) give $\mathbf{v}_s$ at all points on the bubble and wake as a function of ξ. From (31)

$$z - z_c = \frac{1}{U} \int_{(w_s)_c}^{w_s} \exp[\tau(w_s)]\, dw_s,$$

where $w_s = (w_s)_c$ at some reference point $z = z_c$. On $\psi_s = 0$, the above gives

$$x + iy - x_c - iy_c = 2 \int_{\xi_c}^{\xi} \exp[\Omega_0(\xi) + i\chi_0(\xi)]\, d\xi,$$

and so the actual boundary is given for various ξ by

$$\left.\begin{aligned} x &= 1 + 2 \int_{-1}^{\xi} [\exp \Omega_0(\xi)] \cos \chi_0(\xi)\, d\xi, \\ y &= 2 \int_{-1}^{\xi} [\exp \Omega_0(\xi)] \sin \chi_0(\xi)\, d\xi, \end{aligned}\right\} \tag{48}$$

where $z_c = 1$ when $\xi_c = -1$, i.e. the leading edge.

The integrals involving $\sin^{-1} t$ are complicated analytically and can be more easily computed numerically. For the purpose of this paper an approximate integration is given in the appendix. The gross features of the fluid flow field will not be changed. A typical observed value for θ_a is approximately $5\pi/6$. This angle varies with the type of particle but only markedly so in exceptional circumstances as, for example, with synclyst‡, where it may be as small as $\pi/3$. With irregular silver sand, angles may vary from $5\pi/6$ but less drastically. Using the fairly rough approximation set out in the appendix, values were found for $\mathbf{v}_s$ and χ_0 for x and y on the $\psi_s = 0$ streamline. U is taken as unity at infinity. In any calculation the $\mathbf{v}_s$ used is that calculated from above multiplied by U. The gross features of the flow field are obtained from this approximate solution. Figure 10 illustrates the bubble shape as compared with a circle using the appendix approximation. The magnitude and direction of the fluid flow is illustrated at certain points on the bubble and free streamline for $U = 2{\cdot}4$. Note that the velocity of the fluid becomes very small on the free streamline as

† Note that $\chi_0(\xi)$ must be monotonic in this range.

‡ A material with very small particles.

the cusp is approached. This clearly substantiates the contention below that the cloud is as illustrated in figures 11 and 12.

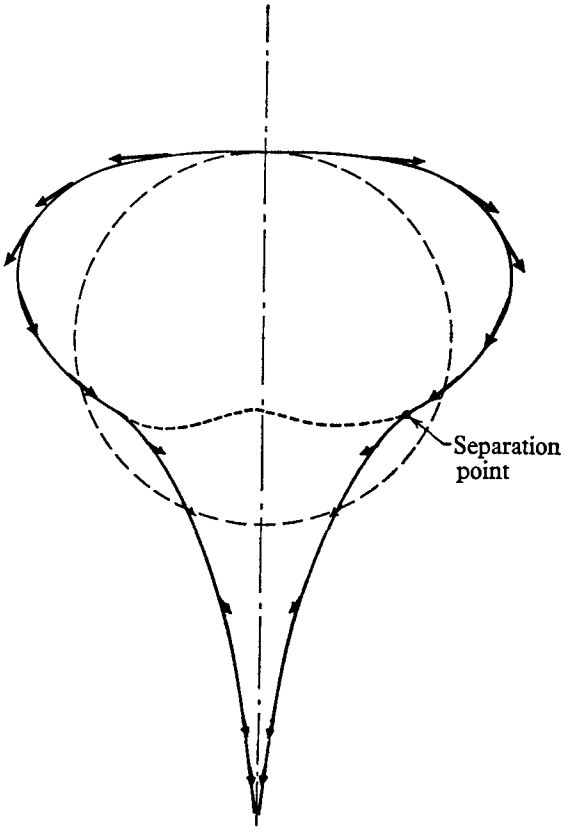

FIGURE 10. Approximate bubble wake shape and fluid flow directions indicated by arrows for $U \doteqdot 2{\cdot}4$.

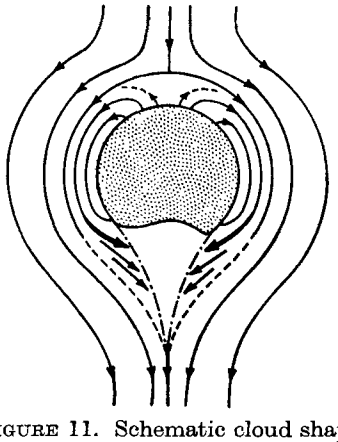

FIGURE 11. Schematic cloud shape in the presence of a wake.

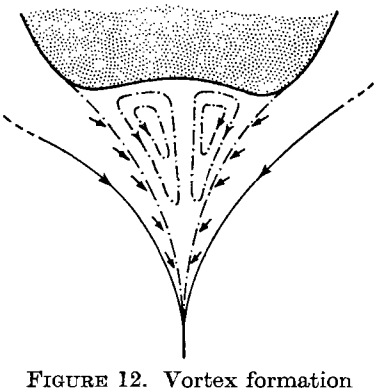

FIGURE 12. Vortex formation in the wake.

We return now to the fluid field obtained from (19). The second of equations (19) gives

$$p - p_0 = -F^{-1}[-cFU^2 + x - cFU^2(v_s)_1],$$

where $(v_s)_1$, $(v_s)_2$ are the components of $\mathbf{v}_s$ in the x- and y- directions. In the vicinity of the leading edge $\mathbf{v}_s$ differs negligibly from that of flow past a circular cylinder. Thus, from the last equation $cFU^2 = 0{\cdot}25$ as in (21). To get the complex potential w_f over the entire field from (19) would involve lengthy and rather unprofitable computations. Since, in general, we are interested in the cloud shape in the vicinity of the wake we can obtain some information by considering ψ_f close to the bubble and wake. For $|\theta| \leqslant \frac{1}{2}\pi$ the cloud shape will be essentially that obtained in §2 above. The cloud is given by $\psi_f = 0$ and the leading edge is given from (15) by the x-value satisfying

$$1 + (v_s)_1 - 0{\cdot}25U^{-1}\,\partial(v_s)_1/\partial x = 0. \tag{49}$$

From (19)

$$\psi_f = y + \psi_s - 0{\cdot}25U^{-1}\,\mathrm{Im}\,(dw_s/dz) = y + \psi_s + 0{\cdot}25U^{-1}v_s \sin\chi. \tag{50}$$

Clearly, in the lower half w_f-plane $\psi_f > 0$ outside the cloud, zero on the cloud and $\psi_f < 0$ inside the cloud. On $\psi_s = 0$, i.e. on the bubble and the free streamline, $(v_s)_2 < 0$, $y < 0$ and so $\psi_f < 0$. In fact, as seen from the table, at *no* point on the bubble or free streamline does $\psi_f = 0$ except at the cusp. More accurate bubbles shapes will not affect this. This holds for all U, since, on $\psi_s = 0$, ψ_s does not depend on U. The cloud therefore joins the wake at the cusp. From figure 11 the fluid velocity decreases on $\psi_s = 0$ as the cusp is approached. The cloud is shown schematically in figure 11. In figure 11 the arrows indicate the direction of the gas flow on the bubble and free streamline.

Ideally the gas going into the wake moves up through the stationary (relative to the bubble) particles and the circulating gas in the cloud persists as a unit of gas and the motion is steady. However, since the direction of the gas flow in the wake tends to carry particles across the free streamline and at the same time induces motion in the wake as illustrated in figure 12, the wake in practice will grow and develop particle vortices. Clearly the motion in the wake will be complicated by the fact that Z may not be equal to unity. While the wake is small enough to be supported by the bubble, the cloud will be symmetrical and similar to that illustrated in figure 5 (*a*). The definite tail is essentially a result in this case of not cutting off the nitrogen dioxide at the exact time. When the wake becomes too large for support by the bubble it becomes unstable and detaches an amount of material which is naturally the vortex unit analogous to casting off of vortices in a real fluid flow past a cylinder. Such a process will naturally be antisymmetric. As we referenced above, these have been regularly observed (Rowe, unpublished). At the moment the particle vortex has been detached the cloud will move in following the new free-streamline shape. This would give the appearance of the cloud moving up in the wake and into the bubble, which is also clear in films of such bubbles in a bed. The lop-sided nature of the cloud would then compensate by allowing a section of the cloud to be detached on the same side as the particle vortex. Once this motion has started the vortices and following cloud sections appear first on one side and then the other. Such a motion is

highly unsteady. However, starting with the mathematically steady motion derived in this section, such an unsteady motion is a natural consequence. These vortices and accompanying cloud sections are very much in evidence experimentally (cf. figure 5(*b*)). The cloud sections are clearly marked in figures 5(*a*) and (*b*). Such patterns as observed there are fairly regular, as the bubbles move up through the bed.

4. Fully developed bubble: three-dimensional case

In the case when there is no wake, no new point arises in the three-dimensional theory. Equations (15)–(18) obtain and the motion is irrotational. If we use the scalar potentials ϕ_f, ϕ_s for the fluid and solids respectively, then (excluding the free stream),

$$\left.\begin{matrix}\phi_f\\ \phi_s\\ p\end{matrix}\right\} = \sum_0^\infty \left.\begin{matrix}f_m\\ s_m\\ p_m\end{matrix}\right\} \frac{P_m(\cos\theta)}{r^{m+1}},$$

where P_m is the Legendre polynomial of order m and f_m, s_m, p_m are constants determined by recurrence relations from equations (17) and (18).

In the case of a circular bubble $r = 1$, we take

$$\phi_s = -U\cos\theta(r + 1/2r^2), \tag{51}$$

and the recurrence relations give f_m and p_m resulting in

$$\left.\begin{aligned}\phi_f &= (1-U)\cos\theta[r - U/2(1-U)r^2] - cFU^2P_2(\cos\theta)/r^3,\\ p - p_0 &= -r\cos\theta/F + cU^2P_2(\cos\theta)/r^3.\end{aligned}\right\} \tag{52}$$

As above, if the coefficient of θ^2 in $p - p_0$ is zero, we get

$$cFU^2 = \tfrac{1}{3}. \tag{53}$$

If we use the same criterion as discussed in § 2 to obtain c we find $c = \frac{3}{5}$. Figure 13 illustrates the velocity curve with this value of c and the experimental results from recent X-ray pictures of bubbles by the techniques set out by Rowe *et al.* (1962). With this more exact technique of measurement, c may be evaluated empirically with fair accuracy and as mentioned above c is a function of F which increases with F only slightly. When F is between 1 and 2, c is equal to $0{\cdot}6 \pm 0{\cdot}02$.

From (52) the flow patterns are seen to be similar to those discussed in § 2, there being a cloud when $U > 1$. Figure 14 gives the ratio of this cloud to bubble diameter as U varies. As in the two-dimensional case the diameter of the cloud is taken to be the width at $\theta = \frac{1}{2}\pi$. With r_c defined in a similar way as in § 2 a figure comparable to figure 6(*b*) would be obtained in this case.

A wake exists in this case and by analogy will form a ring vortex. This vortex will be cast off in a similar manner to that in the two-dimensional case, but without the asymmetry. In a study of particle movement by Rowe & Partridge (1962) the vortex is exhibited by passing a single bubble up through a bed in which the lower half was initially filled with coloured particles. The ring vortex is very distinct.

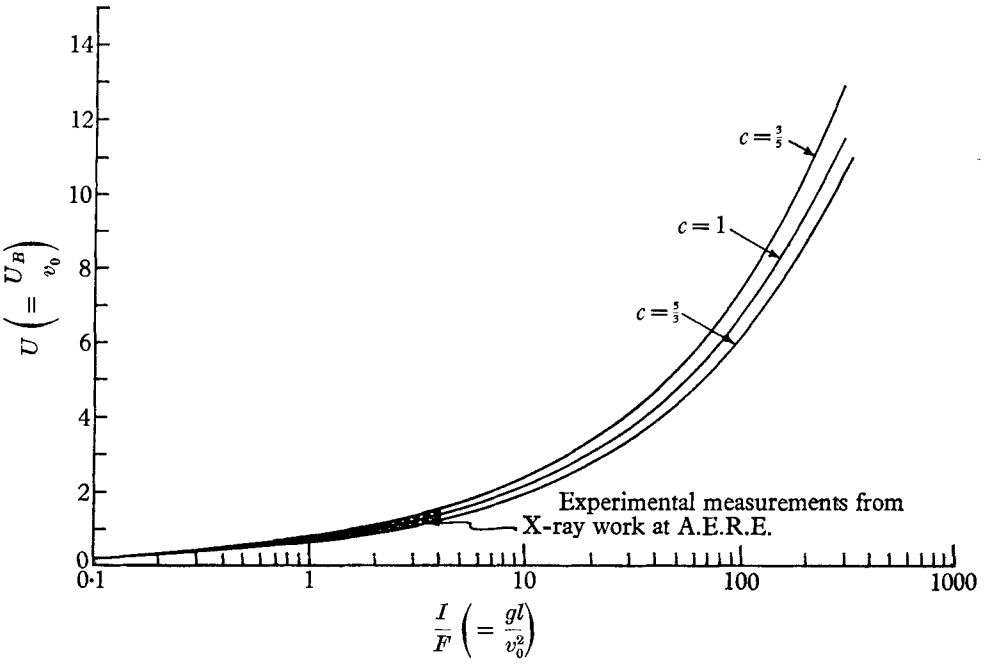

FIGURE 13. Bubble velocity against the Froude number (three-dimensional). Experiments: ballotini–air systems, $R = O(10^3)$.

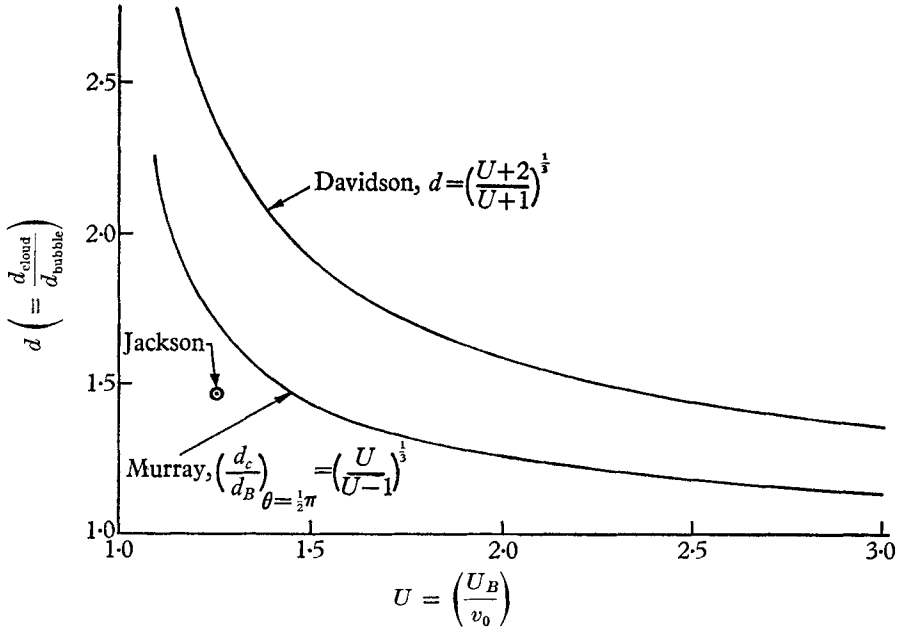

FIGURE 14. Ratio of cloud to bubble diameter againse U (> 1) (three-dimensional).

5. Conclusions

Using the equations of conservation of mass and momentum derived in §2 of part 1 (1965) in the case where the density ratio of solids to fluids is very large an inviscid continuum approximate set of equations are shown to be adequate for the gross description of bubble motion. Using these 'inviscid' (i.e. we omit the solids stress tensor) equations and a modified Oseen technique, solutions are found which exhibit many of the observable features which occur when fully developed bubbles rise up through a fluidized bed. The results are in qualitative agreement with experiment.

The study of the particle flow past a cylinder including a closed free-streamline wake results in flow patterns which suggest reasons for the appearance of particle vortex-like patterns behind the bubble and the actual observed cloud shape when this happens.

It is still an open question as to why the bubbles should be the shapes they are, but justification at this stage for taking them as such is given by the close comparison between the resulting derived flow patterns and the experimental evidence.

For practical engineering purposes equations (15) (or (16)), (17) and (18) suffice, and should adequately describe phenomena such as gross bubble motion and consequently the resulting gross particle motion.

I wish to thank Dr P. N. Rowe of the Chemical Engineering Division, A.E.R.E., Harwell, for the benefit of many most useful discussions, his wide experience of fluidization and for supplying the photographs and most of the experimental results referred to in this paper. I wish also to thank Mr B. A. Partridge of the same Division at Harwell for his assistance in organizing and carrying out the numerical calculations and for many helpful discussions.

Part of this work was carried out under a National Science Foundation Grant GP 2226.

Appendix: approximate evaluation of the integrals appearing in §3

We approximate $\sin^{-1}t$, over the range of integration, by writing

$$\pi^{-1}\sin^{-1}t = A + B(\xi_a - t)^{\frac{1}{2}} + C(\xi_a - t)^{\frac{1}{2}}(\xi_b - t)^{\frac{1}{2}}, \tag{A 1}$$

and we require A and B, and C to be chosen so that equation (A 1) is satisfied at $t = \xi_a$, $t = 0$, and $t = -1$. Thus

$$\left.\begin{aligned} A &= \pi^{-1}\sin^{-1}\xi_a, \\ B &= [(\xi_a\xi_b)^{\frac{1}{2}} - 2A\{(\xi_a+1)^{\frac{1}{2}}(\xi_b+1)^{\frac{1}{2}} - (\xi_a\xi_b)^{\frac{1}{2}}\}][2\xi_a^{\frac{1}{2}}(\xi_a+1)^{\frac{1}{2}}\{(\xi_b+1)^{\frac{1}{2}} - \xi_b^{\frac{1}{2}}\}]^{-1}, \\ C &= [2A\{(\xi_a+1)^{\frac{1}{2}} - \xi_a^{\frac{1}{2}}\} - \xi_a^{\frac{1}{2}}][2\xi_a^{\frac{1}{2}}(\xi_a+1)^{\frac{1}{2}}\{(\xi_b+1)^{\frac{1}{2}} - \xi_b^{\frac{1}{2}}\}]^{-1}. \end{aligned}\right\} \tag{A 2}$$

The integrals in (40) and (45) are obtained from those in (46) and (47) by obtaining the asymptotic forms for large ξ and so will be obtained in the same way below. For convenience introduce

$$D = \left(\frac{\xi_b - \xi}{\xi_a - \xi}\right)^{\frac{1}{2}}, \quad E = \left(\frac{\xi_b - \xi}{\xi - \xi_a}\right)^{\frac{1}{2}}, \quad F = \left(\frac{\xi_b + 1}{\xi_a + 1}\right)^{\frac{1}{2}}, \tag{A 3}$$

where D, E will have the range of ξ which keeps them real. When (A 1) is used in (46), (47) the following integrals arise:

$$\left.\begin{aligned}\int_{-1}^{\xi_a}\left(\frac{\xi_b-t}{\xi_a-t}\right)^{\frac{1}{2}}\frac{dt}{t-\xi} &= D\log\left|\frac{D+F}{D-F}\right|-\log\left(\frac{F+1}{F-1}\right), \quad \text{for} \quad \xi_b<\xi,\xi<\xi_a,\\ &= 2E\tan^{-1}(F/E)-\pi E-\log\{(F+1)/(F-1)\}, \quad \text{for} \quad \xi_a<\xi<\xi_b.\end{aligned}\right\} \tag{A 4}$$

$$\left.\begin{aligned}\int_{-1}^{\xi_a}\frac{(\xi_b-t)^{\frac{1}{2}}}{t-\xi}dt &= 2[(\xi_b-\xi_a)^{\frac{1}{2}}-(\xi_b+1)^{\frac{1}{2}}]\\ &\quad+2(\xi-\xi_b)^{\frac{1}{2}}\left[\tan^{-1}\left(\frac{\xi_b+1}{\xi-\xi_b}\right)^{\frac{1}{2}}-\tan^{-1}\left(\frac{\xi_b-\xi_a}{\xi-\xi_b}\right)^{\frac{1}{2}}\right],\\ &\qquad\qquad \text{for} \quad \xi_b<\xi,\\ &= 2[(\xi_b-\xi_a)^{\frac{1}{2}}-(\xi_b+1)^{\frac{1}{2}}]\\ &\quad-(\xi_b-\xi)^{\frac{1}{2}}\log\left|\frac{[(\xi_b-\xi_a)^{\frac{1}{2}}+(\xi_b-\xi)^{\frac{1}{2}}][(\xi_b+1)^{\frac{1}{2}}-(\xi_b-\xi)^{\frac{1}{2}}]}{[(\xi_b-\xi_a)^{\frac{1}{2}}-(\xi_b-\xi)^{\frac{1}{2}}][(\xi_b+1)^{\frac{1}{2}}+(\xi_b-\xi)^{\frac{1}{2}}]}\right|,\\ &\qquad\qquad \text{for} \quad \xi<\xi_b.\end{aligned}\right\} \tag{A 5}$$

$$\int_{-1}^{\xi_a}\left(\frac{\xi_b-t}{t-\xi}\right)dt = -(\xi_a+1)+(\xi_b-\xi)\log\left|\frac{\xi-\xi_a}{\xi+1}\right|, \quad \text{for all } \xi. \tag{A 6}$$

Equation (45) gives, (using the above, or using (47) with the above integrals and requiring no singularity at $\xi=\xi_b$),

$$\Omega_s = A\log\{(F+1)/(F-1)\}+2B[(\xi_b+1)^{\frac{1}{2}}-(\xi_b-\xi_a)^{\frac{1}{2}}]+C(\xi_a+1), \tag{A 7}$$

after a little manipulation. Substitution of (A 4), (A 5), (A 6) in (47) and letting $\xi\to-1\pm\epsilon$, where $\epsilon\ll 1$, we get

$$\Omega_0(-1\pm\epsilon)\approx(\log\epsilon)[A+B(\xi_a+1)^{\frac{1}{2}}+C(\xi_a+1)^{\frac{1}{2}}(\xi_b+1)^{\frac{1}{2}}] = -\tfrac{1}{2}\log\epsilon,$$

which gives the correct half-power singularity in v_s.

Equation (40) or the appropriate asymptotic form of (A 4) to (A 6) gives the second relation between Ω_s and ξ_b, namely,

$$\begin{aligned}\Omega_s = {} & A\log\{(F+1)/(F-1)\}+2A(\xi_a+1)^{\frac{1}{2}}(\xi_b+1)^{\frac{1}{2}}(\xi_b-\xi_a)^{-1}\\ & +\tfrac{4}{3}B[(\xi_b+1)^{\frac{3}{2}}-(\xi_b-\xi_a)^{\frac{3}{2}}](\xi_b-\xi_a)^{-1}\\ & +C[(\xi_b+1)^2-(\xi_b-\xi_a)^2](\xi_b-\xi_a)^{-1}.\end{aligned} \tag{A 8}$$

Equations (A 7) and (A 8) determine Ω_s and ξ_b for any ξ_a. Substitution of (A 4)–(A 8) together with A–F from (A 1)–(A 3) into (46) and (47) gives $\chi_0(\xi)$, $\Omega_0(\xi)$ as functions of ξ. With these functions the shape of the approximate bubble is given by (48).

The approximation is fairly rough as given in (A 1) but it may be easily improved systematically. However, if accuracy is required in the bubble shape the integrals should be computed exactly.

The case considered is that in which $\theta_a=\frac{5}{6}\pi$, which gives $\xi_a=0{\cdot}8667$. Equations (A 2), (A 7) and (A 8) give

$$\left.\begin{aligned}&\Omega_s = 0{\cdot}3048, \quad \xi_b = 1{\cdot}6900,\\ &A = 0{\cdot}3333, \quad B = 0{\cdot}6059, \quad C = -0{\cdot}7410.\end{aligned}\right\} \tag{A 9}$$

ξ, v_s and χ_0 were calculated for various points and the streamline $\psi_s = 0$ is illustrated in figure 9. The magnitude and direction of the fluid flow for $U = 2{\cdot}4$ is shown at various points on the bubble and wake using (19).

REFERENCES

COLLINS, R. 1965 *Chem. Eng. Sci.* (in the press).

DAVIDSON, J. F. 1961 *Trans. Inst. Chem. Engrs*, **39**, 230.

DAVIDSON, J. F. & HARRISON, D. 1963 *Fluidised Particles*. Cambridge University Press.

DAVIES, R. M. & TAYLOR, G. I. 1950 *Proc. Roy. Soc.* A, **200**, 375.

JACKSON, R. 1963 *Trans. Inst. Chem. Engrs*, **41**, 13.

LEWIS, J. A. & CARRIER, F. G. 1949 *Quart. Appl. Math.* **7**, 228.

MURRAY, J. D. 1963 *Harvard University, Div. Engng Appl. Phys. Tech. Rep.* 1, National Science Foundation Grant GP-2226.

MURRAY, J. D. 1965 *J. Fluid Mech.* **21**, 337.

ROWE, P. N. & PARTRIDGE, B. A. 1962 *Symposium on Fluid/Particle Interactions, 3rd Congress European Fed. Chem. Engng (London)*.

ROWE, P. N., PARTRIDGE, B. A., LYALL, E. & ARDRAN, G. M. 1962 *Nature, Lond.*, **195**, 278.

ROWE, P. N., PARTRIDGE, B. A. & LYALL, E. 1964 *Chem. Eng. Sci.* **19**, 973.

WACE, P. F. & BURNETT, S. J. 1961 *Trans. Inst. Chem. Engrs*, **39**, 168.

WOODS, L. C. 1961 *The Theory of Subsonic Plane Flow*. Cambridge University Press.